Khulna University Studies, 8(1): 151-160, 2007

RESEARCH ARTICLE **PHYSICAL SCIENCE**

STEADY AND UNSTEADY SOLUTIONS OF THE THERMAL FLOWS THROUGH A CURVED DUCT

R.N. Mondal[1*], M.A. Huda[1] and D. Tarafder[2]

[1]*Mathematics Discipline; Science, Khulna University, Khulna 9208, Bangladesh*

[2]*Computer Science and Engineering Discipline; Khulna University, Khulna 9208, Bangladesh*

KUS –07/03-140207

Manuscript received: February 14, 2006; Accepted: April 10, 2007

Abstract: Steady and unsteady solutions of the thermal flows through a curved duct with various aspect ratios are numerically studied by using the spectral method over a wide range of the Dean number, *Dn*. A temperature difference is applied across the vertical sidewalls for the Grashof number *Gr* = 100, 500 and 1000, where the outer wall is heated and the inner wall is cooled. Firstly, steady solutions are obtained by the Newton-Raphson iteration method. As a result, we obtain multiple branches of steady solutions with multi-vortex solutions on various branches. Then, we perform time evolution calculations with a view to study the non-linear behavior of the unsteady solutions. It is found that time periodic solutions appear when *Dn* or *Gr* is increased. If they are increased further, the chaotic solution is obtained. For large aspect ratios, however, chaotic solutions occur for small *Dn* or for small *Gr*.

Key words: Curved duct, thermal flows, steady solutions, dean number, Grashof number

Introduction

The study of flows through a curved duct is of fundamental interest because of its ample applications in fluids engineering, such as in air conditioning systems, refrigeration, heat exchangers, ventilators, and the blade-to-blade passages in modern gas turbines. Blood flow in human veins and arteries is another important application of the curved duct flows. The flow through a curved duct shows physically interesting feature under the action of the centrifugal force caused by the curvature of the duct. The presence of curvature generates centrifugal forces which act at right angle to the main flow direction and produce secondary flows. Dean (1927) was the first who formulated the problem in mathematical terms under the fully developed flow condition. He found the secondary flow consisting of a pair of counter rotating vortices caused by the centrifugal force. Since then, there have been a lot of theoretical and experimental works concerning this flow. Berger *et al*. (1983), Nandakumar and Masliyah (1986) and Ito (1987) may be referred to for some outstanding reviews on curved duct flows.

One of the interesting phenomena of the flow through a curved duct is the bifurcation of the flow because generally there exist many steady solutions due to channel curvature. Dennis and Ng (1982) and Nandakumar and Masliyah (1982) studied dual solutions of the flow through a curved

* Corresponding author: Tel.: 88-041-720171/extn. 265; Fax.: +88-041-731244; e-mail: <rnmondal71@yahoo.com>

DOI: https://doi.org/10.53808/KUS.2007.8.1.0703-PS

duct. Yang and Keller (1986) studied the bifurcation of the flow for small curvature and found multiple branches of solutions. An early bifurcation structure and linear stability of the steady solutions for fully developed flows in a curved square duct was investigated by Winters (1987). He applied bifurcation analysis to it and found that there are many symmetric and asymmetric steady solutions among which linearly stable ones are few. However, the existence of the multiple solutions of the flow through a curved duct with the large aspect ratio was first studied by Yanase and Nishiyama (1988). They obtained two kinds of solutions: the two-vortex solution and the four-vortex solution for the same aspect ratio. Wang and Yang (2004) performed a numerical study on fully developed bifurcation structure and stability of the forced convection in a curved square duct flow. Very recently, Mondal *et al*. (2006) performed numerical prediction of non-isothermal flows through a curved square duct with the effects of curvature. However, complete bifurcation structure as well as transient behavior of the unsteady solutions for both the thermal and non-thermal flows through a curved duct were performed by Mondal (2006).

One of the most important applications of curved duct flow is to enhance the thermal exchange between two sidewalls, because it is possible that the secondary flow may convey heat and then increases heat flux between two sidewalls. Chandratilleke and Nursubyakto (2003) presented numerical calculations to describe the secondary flow characteristics in the flow through curved ducts of aspect ratios ranging from 1 to 8 that were heated on the outer wall, where they studied for small Dean numbers and compared the numerical results with their experimental data. Recently, Yanase *et al*. (2005a) performed numerical investigation of thermal (Gr = 100) and non-thermal flows (Gr = 0) through a curved rectangular duct with differentially heated vertical sidewalls, where they obtained many branches of steady solutions and addressed the time-dependent behavior of the unsteady solutions. In the succeeding paper, Yanase *et al*. (2005b) studied the bifurcation structure as well as the effects of secondary flows on convective heat transfer for moderate Grashof numbers. However, complete bifurcation structure as well as transient behavior of the unsteady solutions for the Dean approximation are yet unresolved, which is important from both engineering and scientific point of view.

In the present paper, numerical results are presented for the fully developed two-dimensional flow of viscous incompressible fluid through a curved duct with differentially heated vertical sidewalls and for various aspect ratios. The aim of the paper is to investigate the flow characteristics with the investigation of time-dependent behavior of the unsteady solutions.

Materials and Methods

Basic equations: Consider a hydrodynamically and thermally fully developed two-dimensional (2-D) flow of viscous incompressible fluid through a curved duct with a constant curvature. The cross section of the duct is a rectangle with width $2d$ and height $2h$. It is assumed that the outer wall of the duct is heated while the inner one is cooled. The temperature of the outer wall is $T_0 + \Delta T$ and that of the inner wall is $T_0 - \Delta T$, where $\Delta T > 0$. The x, y and z axes are taken to be in the horizontal, vertical, and axial directions, respectively. It is assumed that the flow is uniform in the axial direction (i.e. in the z direction), and that it is driven by a constant pressure gradient G along the center-line of the duct, that is, the main flow in the axial direction as shown in Fig. 1.

The variables are non-dimensionalized by using of the representative length d, the representative velocity $U_0 = \nu / d$, where ν is the kinematic viscosity of the fluid. We introduce the non-dimensional variables defined as

$$u=\frac{u'}{U_0},\ v=\frac{v'}{U_0},\ w=\frac{\sqrt{2\delta}}{U_0}w',\ x=\frac{x'}{d},\ \bar{y}=\frac{y'}{d},\ z=\frac{z'}{d}$$

$$T=\frac{T'}{\Delta T},\ t=\frac{U_0}{d}t',\ \delta=\frac{d}{L},\ P=\frac{P'}{\rho {U_0}^2}$$

where u, v and w are the non-dimensional velocity components in the x, y and z directions, respectively; t is the non-dimensional time, P the non-dimensional pressure, δ the non-dimensional curvature defined as $\delta=\frac{d}{L}$, and temperature is non-dimensionalized by ΔT. In the above method of non-dimensionalization, the variables with prime denote the dimensional quantities. Since the flow field is uniform in the z-direction, the sectional stream function ψ is introduced as follows:

$$u=\frac{1}{1+\delta x}\frac{\partial\psi}{\partial y},\quad v=-\frac{1}{1+\delta x}\frac{\partial\psi}{\partial x}$$

We introduce a new coordinate variable y in the $\bar{y}$-direction as $\bar{y}=ly$, where $l=h/d$ is the aspect ratio of the cross section. Then basic equations for w, ψ and T are derived from the Navier-Stokes equations and the heat-conduction equation with the Boussinesq approximation as:

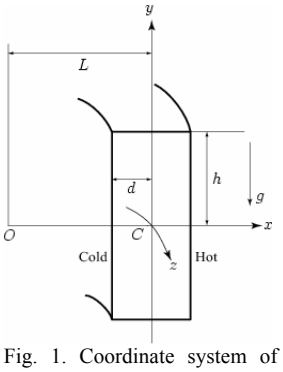

Fig. 1. Coordinate system of the curved rectangular duct.

$$(1+\partial x)\frac{\partial w}{\partial t}+\frac{1}{l}\frac{\partial(w,\psi)}{\partial(x,y)}-D_n+\frac{\delta^2}{(1+\delta x)}=(1+\delta x)\Delta_2 w-\frac{1}{l}\frac{\delta}{(1+\delta x)}\frac{\partial\psi}{\partial y}w+\delta\frac{\partial w}{\partial x},\qquad(2)$$

$$\left(\Delta_2-\frac{\delta}{1+\delta x}\frac{\partial}{\partial x}\right)\frac{\partial\psi}{\partial t}=-\frac{1}{l}\frac{1}{1+\delta x}\frac{\partial(\Delta_2\psi,\psi)}{\partial(x,y)}+\frac{1}{l}\frac{\delta}{(1+\delta x)^2}$$
$$\times\left[\frac{\partial\psi}{\partial y}\left(2\Delta_2\psi-\frac{3\delta}{1+\delta x}\frac{\partial\psi}{\partial x}+\frac{\partial^2\psi}{\partial x^2}\right)-\frac{\partial\psi}{\partial x}\frac{\partial^2\psi}{\partial x\partial y}\right]+\frac{\delta}{(1+\delta x)^2}\left[3\delta\frac{\partial^2\psi}{\partial x^2}-\frac{3\delta^2}{1+\delta x}\frac{\partial\psi}{\partial x}\right]$$
$$-\frac{2\delta}{(1+\delta x)}\frac{\partial}{\partial x}\Delta_2\psi+\frac{1}{l}w\frac{\partial w}{\partial y}+\Delta_2^2\psi-Gr(1+\delta x)\frac{\partial T}{\partial x},\qquad(3)$$

$$\frac{\partial T}{\partial t}+\frac{1}{l}\frac{1}{1+\delta x}\frac{\partial(\psi,T)}{\partial(x,y)}=\frac{1}{\mathrm{Pr}}\left(\Delta_2 T+\frac{\delta}{1+\delta x}\right),\qquad(4)$$

where

$$\Delta_2\equiv\frac{\partial^2}{\partial x^2}+\frac{1}{l^2}\frac{\partial^2}{\partial y^2},\quad \frac{\partial(f,g)}{\partial(x,y)}\equiv\frac{\partial f}{\partial x}\frac{\partial g}{\partial y}-\frac{\partial f}{\partial y}\frac{\partial g}{\partial x}.\qquad(5)$$

Dn, *Gr* and *Pr*, which appear in Eqs. (2) - (4) are defined as

$$Dn=\frac{Gd^3}{\mu\nu}\sqrt{\frac{2d}{L}},\quad Gr=\frac{\gamma g\Delta T d^3}{\nu^2},\quad \mathrm{Pr}=\frac{\nu}{\kappa}.\qquad(6)$$

where μ, γ, κ and g are the viscosity, the coefficient of thermal expansion, the coefficient of thermal diffusivity and the gravitational acceleration, respectively. G is the pressure gradient along the duct axis and is taken to be positive. In the present study, *Dn, Gr* and l vary, while δ and *Pr* are fixed as $\delta = 0.1$ and *Pr* = 7.0 (water).

The rigid boundary conditions for w and ψ are

$$w(\pm 1, y) = w(x, \pm 1) = \psi(\pm 1, y) = \psi(x, \pm 1) = \frac{\partial \psi}{\partial x}(\pm 1, y) = \frac{\partial \psi}{\partial y}(x, \pm 1) = 0, \tag{7}$$

and the conducting boundary conditions for *T* are assumed as

$$T(1, y) = 1, \; T(-1, y) = -1, \; T(x, \pm 1) = x\,. \tag{8}$$

Numerical methods: In order to solve the Eqs. (2) - (4) numerically, the spectral method is used. This method is thought to be the best numerical method to solve the Navier-Stokes equations as well as the energy equation. Details of this method are discussed in Mondal (2006). By this method the variables are expanded in a series of functions consisting of the Chebyshev polynomials. That is, the expansion functions $\Phi_n(x)$ and $\Psi_n(x)$ are defined as

$$\Phi_n(x) = (1 - x^2) C_n(x), \;\; \Psi_n(x) = (1 - x^2)^2 C_n(x), \tag{9}$$

where $C_n(x) = \cos\left(n \cos^{-1}(x)\right)$ is the n-th order Chebyshev polynomial. $w(x, y, z)$, $\psi(x, y, t)$ and $T(x, y, t)$ are expanded in terms of $\Phi_n(x)$ and $\Psi_n(x)$ as

$$\left.\begin{aligned} w(x, y, z) &= \sum_{m=0}^{M} \sum_{n=0}^{N} w_{mn}(t) \Phi_m(x) \Phi_n(y), \\ \psi(x, y, t) &= \sum_{m=0}^{M} \sum_{n=0}^{N} \psi_{mn}(t) \Psi_m(x) \Psi_n(y), \\ T(x, y, t) &= \sum_{m=0}^{M} \sum_{n=0}^{N} T_{mn}(t) \Phi_m(x) \Phi_n(y) + x, \end{aligned}\right\} \tag{10}$$

where M and N are the truncation numbers in the x- and y-directions, respectively. The expansion coefficients w_{mn}, ψ_{mn} and T_{mn} are then substituted into the basic Eqs. (2), (3) and (4) and the collocation method is applied. As a result, the nonlinear algebraic equations for w_{mn}, ψ_{mn} and T_{mn} are obtained. The collocation points are taken to be

$$\left.\begin{aligned} x_i &= \cos\left[\pi\left(1 - \frac{i}{M+2}\right)\right], \qquad i = 1, \ldots, M+1 \\ y_j &= \cos\left[\pi\left(1 - \frac{j}{N+2}\right)\right], \qquad j = 1, \ldots, N+1 \end{aligned}\right\}. \tag{11}$$

The steady solutions are then obtained by the Newton-Raphson iteration method assuming that all the coefficients are time independent. Finally, in order to calculate the time-dependent solutions, the Crank-Nicolson and Adams-Bashforth methods together with the function expansion (10) and the collocation

method are applied. We performed numerical calculations for *Gr* = 100, 500 and 1000 at *Dn* = 100 and 500 for $l = 1, 2$ and 3.

Resistance coefficient: We use the resistance coefficient λ as one of the representative quantities of the flow state. It is also called the *hydraulic resistance coefficient*, and is generally used in fluids engineering, defined as

$$\frac{P_1^* - P_2^*}{\Delta z^*} = \frac{\lambda}{dh^*}\frac{1}{2}\rho\left\langle w^* \right\rangle^2, \tag{12}$$

where quantities with an asterisk denote dimensional ones, $\langle\ \rangle$ stands for the mean over the cross section of the rectangular duct, and $d_h^* = 4(2d \times 2dl)/(4d + 4dl)$. The mean axial velocity $\left\langle w^* \right\rangle$ is calculated by

$$\left\langle w^* \right\rangle = \frac{v}{4\sqrt{2\delta}ld}\int_{-1}^{1} dx \int_{-1}^{1} \overline{w}(x, y)dy. \tag{13}$$

Since $\left(P_1^* - P_2^*\right)/\Delta z^* = G$, λ is related to the mean non-dimensional axial velocity $\langle w \rangle$ as

$$\lambda = \frac{8l\sqrt{2\delta}Dn}{(1+l)\langle w \rangle^2}, \tag{14}$$

where $\langle w \rangle = \sqrt{2\delta}d\left\langle w^* \right\rangle / v$.

In this paper, we use λ to discriminate steady solution branches and to pursue the time evolution of the unsteady solutions.

Results

Steady solutions*:* We obtain steady solutions of the thermal flows through a curved duct with square and rectangular cross sections. The steady solutions are obtained by the path continuation technique with different initial guesses as discussed in Mondal (2006). We obtain two branches of steady solutions for a square duct, while five and six branches for a rectangular curved duct with aspect ratios 2 and 3, respectively over a wide range of the Dean number (for details please see Mondal, 2006). A bifurcation structure of the steady solutions, for example, is shown in Fig. 2 for *Gr* = 500 and $l = 2$ over the Dean number $100 \le Dn \le 1000$ using λ, the representative quantity of the solutions. It is found that the steady solution branches are independent and there exists no bifurcating relationship among them in the parameter range investigated in this paper. The solution branches are distinguished by the nature and number of secondary flow vortices appearing in the cross section of the duct.

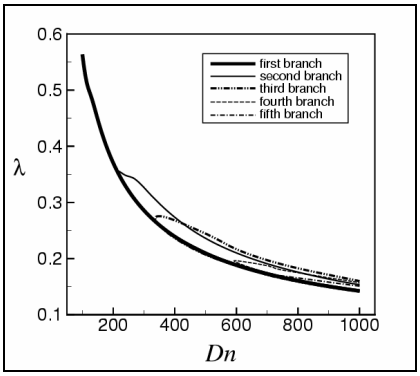

Fig. 2. Steady solution branches for *Gr* = 500, $l = 2$ and $100 \le Dn \le 1000$ (thick solid line: first branch, thin solid line: second branch, dash dot dot line: third branch, dashed line: fourth branch, dash dotted line: fifth branch).

It is found that the first branch contains one- and two-vortex solutions. The second branch consists of two- and four-vortex solutions. The third branch is characterized by two- and four-vortex solutions, but different from the second branch in the form of vortices near the outer wall. The fourth branch contains two-, four-, and six-vortex solutions. The fifth branch is composed of two-, four-, six-, eight- and ten-vortex solutions. In this regard, it should be remarked that Yanase *et al.* (2005a) obtained both symmetric and asymmetric steady solutions for the non-thermal flow in a curved rectangular duct. In the present study of thermal flows, however, we obtain only asymmetric steady solutions. The reason is that heating the outer wall causes deformation of the secondary flow and yields asymmetry of the flow.

Unsteady solutions: We study the non-linear behavior of the unsteady solutions by time-evolution calculations of the Eqs. (2) - (4) with a temperature difference between the vertical outer and inner sidewalls. Calculations are performed for $\delta = 0.1$, $\mathrm{Pr} = 7.0$, $Dn = 100$ and 500, $Gr = 100$, 500 and 1000 for $l = 1, 2, 3$. We show the time-evolution of λ for $l = 1$ in Fig. 3(a). In this figure, a thick solid line stands for Gr = 100, a thin solid line for Gr = 500, and a dashed line for Gr = 1000. In the figure, the flow approaches a steady state immediately for all three cases, and λ becomes small if Gr is increased. We show the secondary flow patterns and the

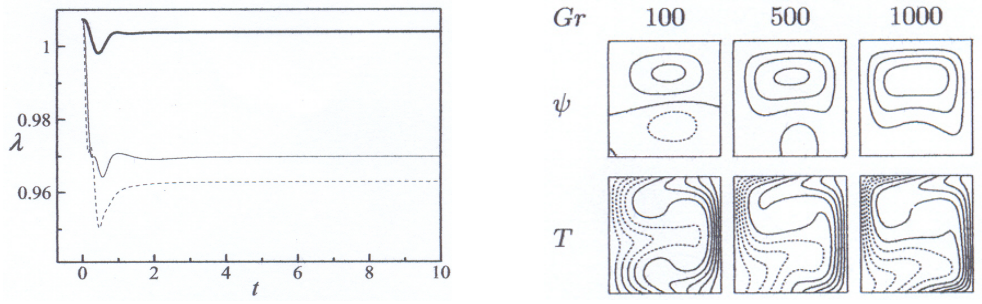

(a) (b)

Fig. 3. (a) Time-evolution of λ with the thermal effect for Dn = 100 and l = 1 (thick solid line: Gr = 100, thin solid line: Gr = 500, dashed line: Gr = 1000). (b) Secondary flow patterns (top) and temperature distributions (bottom) for Dn = 100 and l = 1 at t = 10.

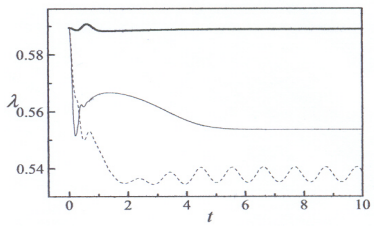

Fig. 4. Time-evolution of λ with the thermal effect for Dn = 100 and l = 2 (thick solid line: Gr = 100, thin solid line: Gr = 500, dashed line: Gr = 1000).

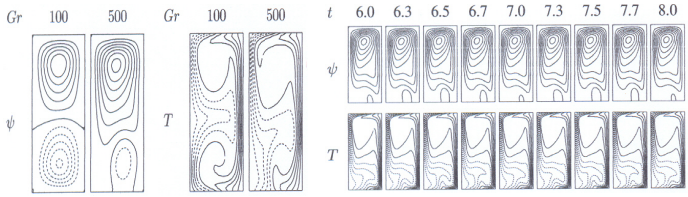

(a) (b)

Fig. 5. (a) Secondary flow patterns (left) and temperature distributions (right) for Dn = 100, l = 2 and Gr = 100, 500 at t = 10. (b) Secondary flow patterns (top) and temperature distributions (bottom) for Dn = 100, l = 2 and Gr = 1000 for one period of oscillation at $6.0 \le t \le 8.0$.

temperature distributions at t = 10 in Fig. 3(b), where the contours of ψ and T are drawn with the increments $\Delta\psi = 0.8$ and $\Delta T = 0.2$, respectively. The same increments of ψ and T are used for all the figures in this paper, if not specified. In the figures of the secondary flow, solid lines $(\psi \ge 0)$ show that the secondary flow is in the counter clockwise direction while the dotted lines $(\psi < 0)$ in the clockwise direction. Similarly, in the figures of the temperature field, solid lines are those for $T \ge 0$ and dotted ones for $T < 0$. As seen in Fig. 3(b), when Gr becomes large the

symmetry with respect to $y = 0$ breaks. The reason is that the effect of buoyancy force becomes comparable as that of centrifugal force when the temperature difference becomes large.

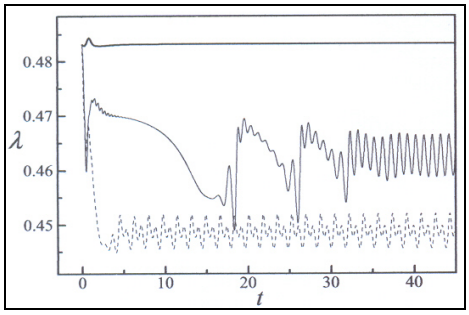

Fig. 6. Time-evolution of λ with the thermal effect for Dn = 100 and l = 3 (thick solid line: Gr = 100, thin solid line: Gr = 500, dashed line: Gr = 1000).

We show the results of time-evolution calculations for $l = 2$ in Fig. 4. As seen in Fig. 4, the flow attains a steady state for Gr =100 and 500, but it oscillates periodically for Gr = 1000. Now we show the secondary flow patterns and the temperature distributions for Gr = 100, 500 at t = 10 in Fig. 5(a) and for Gr = 1000, for one period of oscillation at $6.0 \le t \le 8.0$, in Fig. 5(b). The periodic change is observed in the secondary flow patterns and the temperature distributions as seen in Fig. 5(b). We show the time-evolution results for $l = 3$ in Figs. 6 and 7. At Gr = 500, a periodic oscillation occurs, and at Gr = 1000 a periodic solution consisting with plural periods is observed. Though the symmetry with respect to $y = 0$ is approximately maintained for Gr = 100 (see Fig. 7(a)), it completely disappears if Gr is increased more. In Figs. 7(b) and 7(c), the periodic oscillations of the time-dependent flows are observed. From these results it is found that the oscillation tends to occur when Gr or l increased, if Dn is kept constant.

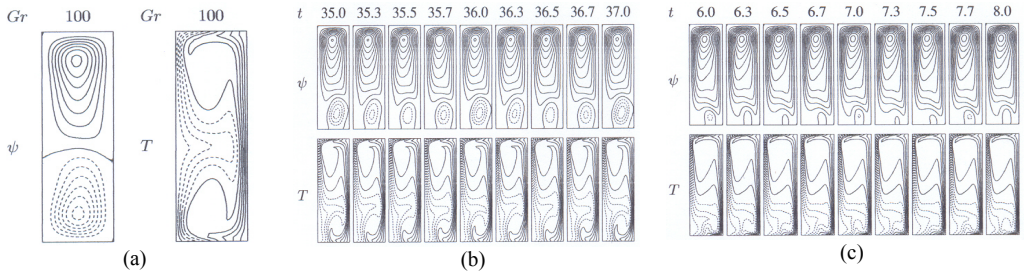

Fig. 7. Secondary flow patterns and temperature distributions. (a) Dn = 100, l = 3 and Gr = 100 at t = 10, (b) Dn = 100, l = 3 and Gr = 500 at $35.0 \le t \le 37.0$, (c) Dn = 100, l = 3 and Gr = 1000 at $6.0 \le t \le 8.0$.

Next, we show results of time-evolution calculations for Dn = 500. We use the steady solution for Dn = 100 as the initial condition. Figure 8(a) shows the results of time-dependent solutions for $l = 1$ and Dn = 500, and 8(b) shows the secondary flow patterns and temperature distributions for $l = 1$ and Dn = 500 at t = 10. Comparing Fig. 8(b) with Fig. 3(b), it is found that the symmetry approximately exists even for large Gr in the case of Dn = 500, because the centrifugal force becomes strong when Dn increases. We show the results of time-evolution calculations along with the secondary flow patterns and temperature distributions for $l = 2$, $Dn = 500$ and Gr = 100 in Figs. 9(a) and 9(b), respectively.

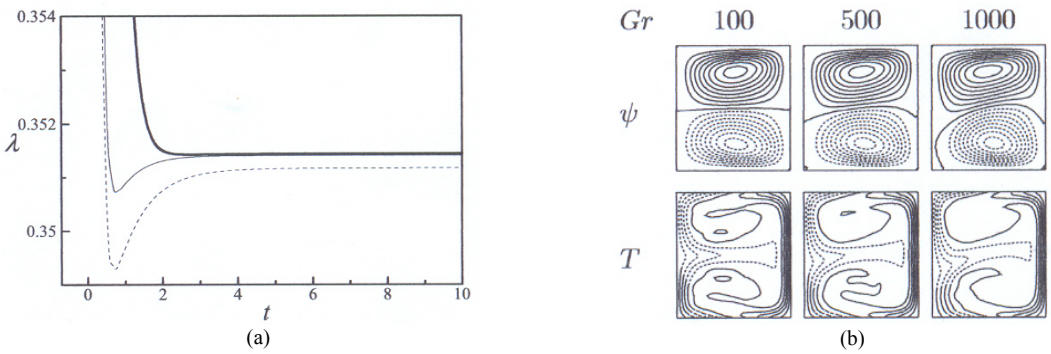

(a) (b)

Fig. 8. (a) Time-evolution of λ with the thermal effect for Dn = 500 and l = 1 (thick solid line: Gr = 100, thin solid line: Gr = 500, dashed line: Gr = 1000). (b) Secondary flow patterns (top) and temperature distributions (bottom) for Dn = 500 and l = 1 at t = 10.

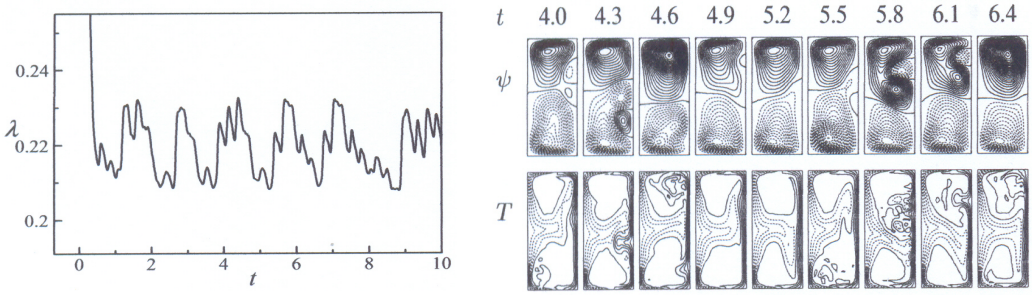

(a) (b)

Fig. 9. (a) Time-evolution of λ with the thermal effect for Dn = 500, Gr = 100 and l = 2. (b) Secondary flow patterns (top) and temperature distributions (bottom) for Dn = 500, Gr = 100 and l = 2 at $4.0 \le t \le 6.4$.

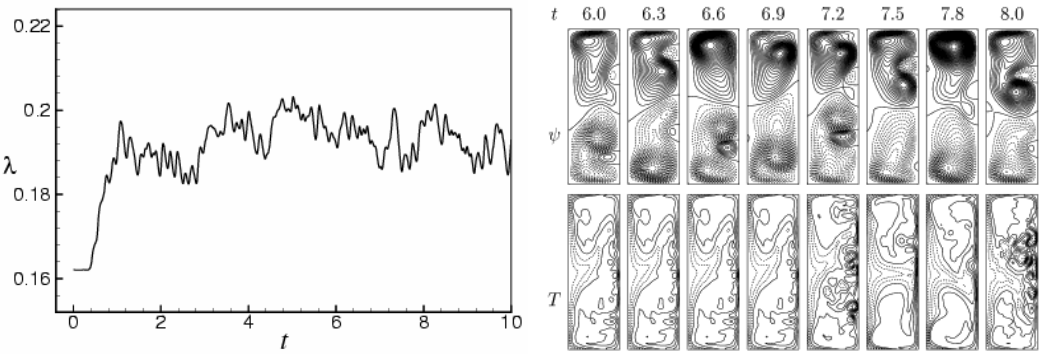

(a) (b)

Fig. 10. (a) Time-evolution of λ with the thermal effect for Dn = 500, Gr = 100 and l = 3. (b) Secondary flow patterns (top) and temperature distributions (bottom) for Dn = 500, Gr = 100 and l = 3 at $6.0 \le t \le 8.0$.

As seen in Fig. 9(a), the flow oscillates non-periodically i.e. the flow is chaotic. The secondary flow patterns and temperature profiles for this chaotic oscillation are shown in Fig. 9(b) for $4.0 \le t \le 6.4$. It is found that the chaotic oscillation at Dn = 500, Gr = 100 and l = 2 consists of two- and four-vortex solutions. In this regard, it should be noted that the flow does not oscillate when Dn = 100 and Gr = 100 (Fig. 7), but the flow oscillates when Dn = 500 and Gr =100 (Fig. 9(b)). This result suggests that an oscillation tends to occur when Dn increases. Time-evolution of

λ is then performed for *Dn* = 500, *Gr* = 100 and *l* = 3, as shown in Fig. 10(a). Figure 10(a) shows that the flow oscillates irregularly with large windows of quasi-periodic oscillations which mean that the flow is chaotic. Contours of secondary flow and temperature distribution for the chaotic solution at *Dn* = 500, *Gr* = 100 and *l* = 3 are shown in Fig. 10(b) for $6.0 \le t \le 8.0$. It is found that the chaotic oscillation at *Dn* = 500, *Gr* = 100 and *l* = 3 comprises four- and six-vortex solutions. Thus we observed that, if one of the parameters, *Dn* or *Gr,* is increased up to a certain level, the periodic solution turns into chaotic state. However, for large aspect ratio this transition easily occurs for moderate *Dn* or *Gr*.

Discussion

In the present paper, we have performed two-dimensional calculations to study the curved duct flows, because it has been shown by many experimental and numerical studies that curved duct flows easily attain asymptotic fully developed 2-D states (uniform in the main flow direction) at most 270^0 from the inlet. A recent work by Wang and Yang (2005) shows that even a periodic flow can be analyzed by 2-D calculations. They showed that for an oscillating flow there exists a close similarity between the flow observation at 270^0 and 2-D calculations. In fact, the periodic oscillation, obtained in the present study, represents a three-dimensional traveling wave solution in real flows.

There is some evidence showing that the occurrence of chaotic or turbulent flow may be predicted by 2-D analysis. Yamamoto *et al.* (1998) investigated linear stability of helical pipe flows with respect to 2-D perturbations and compared the results with their experimental data, where they obtained a good agreement between the two results. Thus, the transition from periodic oscillation to the chaotic state, obtained by the 2-D calculation in the present paper, may correspond to the destabilization of travelling waves in the curved duct flows like that of Tollemin-Schlichting waves in a boundary layer. Our 2-D analysis, therefore, may contribute to the study of curved duct flows, because it is difficult to have a good physical insight into the curved duct flows without having 2-D analysis.

Conclusion

We obtained steady solutions of the thermal flows through a curved duct with square and rectangular cross sections over a wide range of the Dean number for the curvature $\delta = 0.1$. We obtained two branches of steady solutions for a square duct, while five and six branches for a rectangular duct of aspect ratios 2 and 3, respectively. The two-, four-, six-, eight- and ten-vortex solutions were obtained on various branches of steady solutions.

Then, we studied the unsteady solutions of the velocity and temperature fields. *Gr*, defined by the temperature difference between two sidewalls, is increased up to 1000 with *Pr* = 7.0. It is found that the larger *Gr* is, the flow loses its symmetry with respect to the plane $y = 0$. For some cases, on the other hand, the symmetry is approximately maintained when *Dn* is increased. Therefore the temperature difference and the pressure gradient along the duct affect the fluid in an opposite manner as for the symmetry of the flow. It is also found that the flow becomes time-dependent and periodic when *Dn* or *Gr* is increased. For this case, two effects affect the fluid in a similar manner. If they are increased further, we observed chaotic solutions. For large aspect ratios, on the other hand, the transition from periodic to chaotic state occurs if *Dn* or *Gr* is small.

References

Berger, S.A.; Talbot, L. and Yao, L.S. 1983. Flow in curved pipes. *Annual Review of Fluid Mechanics,* 35: 461–512.

Chandratilleke, T.T. and Nursubyakto. 2003. Numerical prediction of secondary flow and convective heat transfer in externally heated curved rectangular ducts. *International Journal of Thermal Sciences*, *42*: 187-198.

Dean, W.R. 1927. Note on the motion of fluid in a curved pipe. *Philosophical Magazine,* 4: 208–223.

Dennis, S.C.R. and Ng, M. 1982. Dual solutions for steady laminar flow through a curved tube. *Quarterly Journal of Mechanics and Applied Mathematics,* 35: 305-324.

Ito, H. 1987. Flow in curved pipes. *JSME International Journal*, 30: 543–552.

Mondal, R.N. 2006. Isothermal and non-isothermal flows through curved ducts with square and rectangular cross sections, Ph.D. Thesis, Department of Mechanical Engineering, Okayama University, Japan.

Mondal, R.N.; Kaga, Y.; Hyakutake, T. and Yanase, S. 2006. Effects of curvature and convective heat transfer in curved square duct flows. *ASME Journal of Fluids Engineering*, 128(9): 1013–1023.

Nandakumar, K. and Masliyah, H.J. 1982. Bifurcation in steady laminar flow through curved tubes. *Journal of Fluid Mechanics,* 119: 475-490.

Nandakumar, K. and Masliyah, J.H. 1986. Swirling flow and heat transfer in coiled and twisted pipes. *Advanced Transport Process,* 4: 49–112.

Wang, L. and Yang, T. 2004. Bifurcation and stability of forced convection in curved ducts of square cross section. *International Journal of Heat and Mass Transfer*, 47: 2971-2987.

Wang, L. and Yang, T. 2005. Periodic oscillation in curved duct flows. *Physica D*, 200: 296-302.

Winters, K.H. 1987. A bifurcation study of laminar flow in a curved tube of rectangular cross-section. *Journal of Fluid Mechanics,* 180: 343–369.

Yamamoto, K.; Yanase, S. and Jiang, R. 1998. Stability of the flow in a helical tube. *Fluid Dynamics Research*, 22: 153-170.

Yanase, S. and Nishiyama, K. 1998. On the bifurcation of laminar flows through a curved rectangular tube. *Journal of the Physical Society of Japan,* 57: 3790-3795.

Yanase, S.; Mondal, R.N.; Kaga, Y. and Yamamoto, K. 2005a. Transition from steady to chaotic states of isothermal and non-isothermal flows through a curved rectangular duct. *Journal of the Physical Society of Japan*, 74(1): 345–358.

Yanase, S.; Mondal, R.N. and Kaga, Y. 2005b. Numerical study of non-isothermal flow with convective heat transfer in a curved rectangular duct. *International Journal of Thermal Sciences*, 44(11): 1047–1060.

Yang, Z. and Keller, H.B. 1986. Multiple laminar flows through curved pipes. *Applied Numerical Mathematics*, 2: 257-271.